Limnol. Oceanogr., 53(5, part 2), 2008, 2321–2332

Convectively driven transport in temperate lakes

Alexander L. Forrest and Bernard E. Laval
University of British Columbia, Department of Civil Engineering, 6250 Applied Science Lane, Room 2010, Vancouver, British Columbia V6T 1Z4, Canada

Roger Pieters
University of British Columbia, Department of Earth and Ocean Sciences, 6339 Stores Road, Vancouver, British Columbia V6T 1Z4, Canada

Darlene S. S. Lim
NASA Ames Research Center, Space Science and Astrobiology Division, Building 245, Mail Stop 245-3 Room 283, Moffett Field, California 94035-1000

Abstract

Penetrative convection in the surface layer of a midsize temperate lake (5 km^2) was investigated in both summer and winter using a conductivity–temperature–depth (CTD) logger mounted on an autonomous underwater vehicle (AUV) flown repeatedly along horizontal transects at selected depths. In summer, the epilimnion cooled differentially during a calm evening (240 and 297 W m^{-2} on the east and west sides of the lake, respectively). These cooling rates agree well with the average net heat flux of 270 W m^{-2} estimated from meteorological data. Density currents were driven by this differential cooling. In winter, CTD profiles during a sunny day showed four distinct thermal layers beneath the ice (~50 cm thick), consistent with radiative penetrative convection: a stratified diffusive layer just beneath the ice (top 1.6 m); a well-mixed convective layer (that deepens at 1.14 m d^{-1} and warms at 0.015°C d^{-1} during the observation period); an entrainment layer (1.5 m thick); and a weakly stratified quiescent layer (to bottom). AUV transects, flown at constant depths in each layer, revealed a 150-m wide region displaying evidence of penetrative convection, surrounded by regions with negligible heat changes. These high-resolution, horizontal CTD measurements provided insight into previously unresolved physical dynamics of the well-mixed layer of a temperate lake in quasi–shear-free conditions that would have been difficult to quantify during summer months and impossible under winter ice cover without the use of an AUV platform.

In temperate lakes, during periods of little or no wind exposure, penetrative convection driven by a destabilizing buoyancy flux will be the dominant source of vertical mixing in the upper layers of the water column. Above the temperature of maximum density, penetrative convection occurs during periods of heat loss from the water surface (Wells and Sherman 2001). On a daily timescale, cooling at night results in vertical mixing within the surface layer and can erode a diurnal thermocline (Imberger 1985; Lei and Patterson 2006). Seasonally, autumnal cooling results in the erosion of the seasonal thermocline (Fer et al. 2002*c*; Wells and Wettlaufer 2007). In contrast, below the temperature of maximum density and under ice cover, shortwave solar radiation that penetrates the ice results in convective mixing driven by volumetric solar heating (Farmer 1975; Mironov et al. 2002). Solar heating beneath the ice results in the deepening of a well-mixed layer at a rate that is proportional to the depth of the ice cover (Jonas et al. 2003).

While seasonal penetrative convection on a basin scale has received a fair degree of attention (Imberger 1985; Fer et al. 2002*a*; Jonas et al. 2003), less attention has been given to horizontal and short timescale variability associated with differential heat flux. Exceptions include studies demonstrating higher cooling rates in shallow littoral zones than in adjacent deeper waters (Monismith et al. 1990; Fer et al. 2002*b*). These increased cooling rates result in the formation of both turbulent density currents and convective plumes. A major limitation to the study of horizontal variability on short timescales is that conventional instrumentation is largely designed for vertical, rather than horizontal, sampling.

Within the past decade, autonomous underwater vehicles (AUVs) have seen increased application in physical

Acknowledgments

The Pavilion Lake Research Project and University of British Columbia (UBC) Gavia operations at Pavilion Lake were supported by the Canadian Space Agency Canadian analogue research network (CARN) program, the National Aeronautics and Space Administration (NASA) astrobiology program, the National Geographic Society committee for research exploration (CRE), and the Canadian National Science and Engineering Research Council (NSERC) discovery program. Funding for the purchase of UBC Gavia was provided by the Canadian Foundation for Innovation, the British Columbia Knowledge Development Fund, and the University of British Columbia. Operations at Pavilion Lake would not be possible without the support of the Ts'kw'aylaxw First Nation, the Pavilion Lake Community, Mickey and Linda Macri, Donnie Reid, Dale Andersen, Harry Bohm, and British Columbia Parks. Alexander Forrest was supported by a Canada NSERC postgraduate scholarship-doctorate (PGS-D) scholarship. We also acknowledge the technical support of Richard Yeo and Eggert Magnusson of Hafmynd, Ltd., Iceland and Martin Doble from the University of Cambridge, UK who worked hard to ensure that our under-ice endeavors were successful. This manuscript represents Pavilion Lake Research Project publication 07-01.

oceanography with examples including shallow hydrographic surveys of Narragansett Bay, Rhode Island (Levine et al. 1997); a survey of coastal fronts in Haro Straight, British Columbia (Nadis 1997); deep-water hydrographic and current measurements in the Straight of Sicily (Stansfield et al. 2001); turbulence gradient measurements (Thorpe et al. 2002); water renewal in hypoxic sea lochs (Overnell et al. 2002); and AUV-based acoustic Doppler current profiler (ADCP) flow field measurement (Fong and Jones 2006). To date, there are a few examples of this technology being applied to limnological studies; however some examples of freshwater work include flow field prediction in tidally forced lakes (Fong and Jones 2006), internal waves in a small lake (Laval et al. 2000*a*), and gravity currents associated with littoral cooling (Fer et al. 2002*b*).

An investigation of the horizontal heterogeneity of the thermal structure within the well-mixed layer of a temperate lake was made using University of British Columbia (UBC) Gavia as a platform for high-resolution conductivity–temperature–depth (CTD) measurements. During evening cooling in late summer, and in the absence of significant wind shear, the epilimnion displayed basin-scale variability in mean temperature and cooling rates, which we suggest results from the underlying geometry. In winter, evidence of radiatively driven convection was collected, and we suggest that the observed basin-scale heterogeneity results from variation in ice surface characteristics including total ice thickness, associated optical properties, areal variability of the snow cover (coverage and depth), and sun exposure. Penetrative convection is important in accounting for chemical and biological variability in natural lake systems (Stefanovic and Stefan 2002) and is a fundamental contributor to mass transport in temperate lakes under quasi–shear-free conditions sometimes present during periods of low wind shear in the summer and always present under winter ice cover.

Methods

Site description—The selected deployment site was Pavilion Lake, a 5 km^2, groundwater fed, temperate lake located in central British Columbia in a limestone valley known as Marble Canyon (*see* Fig. 1). Pavilion Lake has three basins (north, central, and south basins) oriented along the longitudinal axis of the lake interconnected with sills 6–10-m deep. All AUV-based work presented in this study was done in the central basin at the widest point of the lake. This work is part of an ongoing study of the benthic regions of this relatively deep (maximum recorded depth of 61 m) freshwater lake, which has evidence of macroscale growth of organosedimentary structures known as microbialites (Laval et al. 2000*b*). One objective of this ongoing study is to examine how mass transport associated with convective processes influences microbialite distribution.

Data collection—High-resolution CTD measurements were made with a Seabird Electronics SBE-49 mounted on UBC Gavia, a small Gavia-class AUV. As configured for freshwater operation, the vehicle is approximately 2.4 m in length, 0.2 m in diameter, and 55 kg dry weight. Although the maximum velocity of the vehicle is approximately 3 m s^{-1}, the selected cruising speed was 1.6 m s^{-1} to provide an along track spatial resolution of 10 cm. The vehicle navigated using a combined RDI workhorse navigator Doppler velocity log (DVL) and a Kearfott inertial navigation system (INS). Since the water column depths exceeded the range of the DVL (>30 m), periodic surface intervals were required to reset accumulated position error. Mission design was to have the vehicle run at constant depths where a tolerance of 10 cm (i.e., $\pm$5 cm away from the depth set point) was considered acceptable; data points exceeding this tolerance are not reported.

The investigation was divided into two campaigns; summer (08–09 August 2006) and winter (21–22 February 2007). The summertime mission objective for UBC Gavia was to repeatedly cycle between a constant depth transect (~500-m long) in the surface mixed layer (2.12-m depth) and then return along the seasonal thermocline (7.02-m depth). In winter, transects (~300-m long) were collected in the stratified surface layer (0.5-m depth), and the convectively mixed layer (6.2- and 17-m depth). During both campaigns, simultaneous Seabird SBE19plus CTD profiles (vertical resolution ca. 20 cm) were collected continuously during vehicle deployment at a fixed location along the mission transects (Fig. 1).

Five ice profiles were collected on 25 February 2007, 3 d after the AUV sampling at the approximate beginning, middle, and end of the AUV transect in the central basin (Fig. 1) and also from the centers of the south and north basins. No precipitation occurred during the interval between AUV and ice sampling. Samples of both the white and black ice were collected in polyethylene bags, melted at room temperature, and then transferred to sample bottles. Melted ice water samples were measured for conductivity using a Guildline Portasal. At each of the holes in the central basin, a YSI 556 MPS multiprobe was used to profile the upper 20 cm of the water column. Measured parameters included pH, dissolved oxygen (DO), conductivity, and temperature. SBE19plus CTD profiles were collected from each of the five holes as well as the sampling holes from the north and south basins.

Meteorological data (wind speed and direction, air temperature, relative humidity, incoming shortwave solar radiation) were measured from a Campbell Scientific CR1000 weather station positioned on the shoreline at a point near the sill separating the north and central basins (*see* Fig. 1a). Wind parameters were sampled every 10 s and then averaged every 15 min, while all other variables were averaged over 30-min intervals. During ice-free conditions, these data, along with the surface water temperature (estimated using the average temperature values from CTD casts during the testing period), are required to estimate the surface heat flux. Near-neutral stability of the atmosphere above the lake surface was assumed (i.e., $z_a/L_o < 0.5$; where z_a is the measurement height above the water surface and L_o is the Monin-Obukhov length in the atmospheric boundary layer), and calculation of the bulk transfer coefficients of the bulk

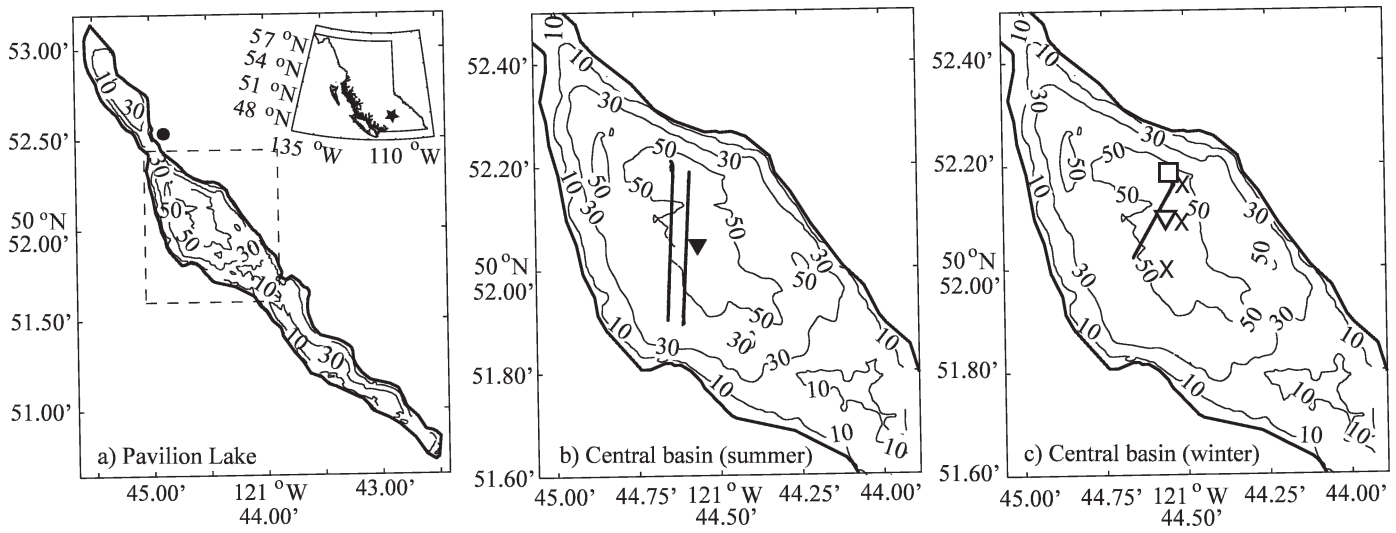

Fig. 1. (a) Bathymetry of Pavilion Lake with British Columbia location inset (filled circle—location of meteorological station). Contours represent 20-m intervals with maximum depth of 61 m in the central basin. The area outlined with a dashed line is enlarged in panels b and c. (b) Summertime AUV transects (solid lines): transect in mixed layer (2.12-m depth) on left and transect along the thermocline (7.02-m depth) on right (filled inverted triangle—location of vertical CTD profiling). (c) Wintertime AUV transect (solid line) for all depths (open square—point of launch and recovery; open inverted triangle—site of vertical CTD profiling; X—three locations of ice profiling).

aerodynamic formulae was solved iteratively to estimate the latent and sensible heat flux rates (Launiainen 1995; Launiainen and Cheng 1998; Heikinheimo et al. 1999).

Results and discussion

Summertime campaign (cooling heat flux)—Vertical CTD profiles were collected before and during the AUV-mounted CTD transects to determine the vertical variability in the background stratification. Since the transect repeat interval of the AUV was significantly greater than the dissipation time of the relatively low amounts of kinetic energy induced by the CTD, it was concluded that the horizontal profiling was not skewed by the vertical profiles. On 09 August 2006, 138 consecutive vertical CTD profiles were collected in the approximate center of the AUV track (*see* Fig. 1b). Figure 2 shows that the seasonal thermocline depth (where $|\partial T/\partial z|$ is a maximum) remains stable at a value of 6.86 ± 0.27 m. The surface mixing layer, *h,* is defined as being where $\partial T/\partial z \approx 0$, and the variation in temperature due to internal waves is small—taken here as h ~4.0 m (Fig. 2). The mean vertical temperature gradient values at the depth of the shallow (2.12 ± 0.05 m) and deep (7.02 ± 0.05 m) AUV transects were (25.6 ± 0.07) × 10^{-2} K m^{-1} and 1.97 ± 0.02 K m^{-1}, respectively (ranges represent one standard deviation). If we combine these mean vertical temperature gradients with the ±5 cm tolerance of the AUV depth set point, scales for temperature changes associated with vertical displacements of the AUV are estimated as (2.56 ± 0.02) × 10^{-3}°C and (1.97 ± 0.05) × 10^{-1}°C for the shallow and deep transects, respectively.

The AUV-mounted CTD profiled horizontally 13 times alternating between two depths. We first discuss the data collected at 2.12 ± 0.05 m depth. In the first transect, 10-m bin-averaged temperature increased from 19.1°C at the reference point to 19.2°C at the other end of the transect (far from reference point; Fig. 3). At the end of the experiment, the temperature along the transect was near constant at about 18.95°C.

The heat flux required to account for the observed cooling of the surface mixing layer ($\tilde{H}$) can be estimated by vertically integrating the change in heat content (Moni-

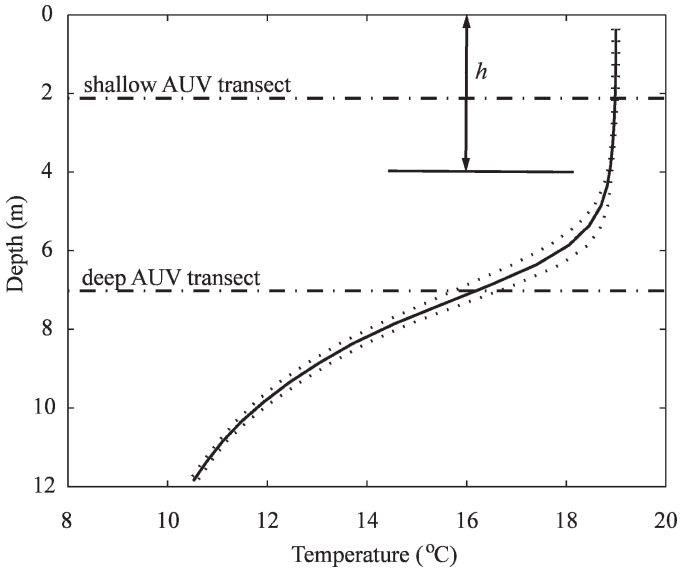

Fig. 2. Bin-averaged temperature profiles: solid line—average temperature over testing period on 09 August 2006 (n = 138, bin size = 0.5 m); dotted lines—standard deviation of averaged temperature profiles; dashed-dot lines at 2.12- and 7.02-m depths indicate shallow and deep AUV transect depths, respectively (h is the depth of the surface mixed layer).

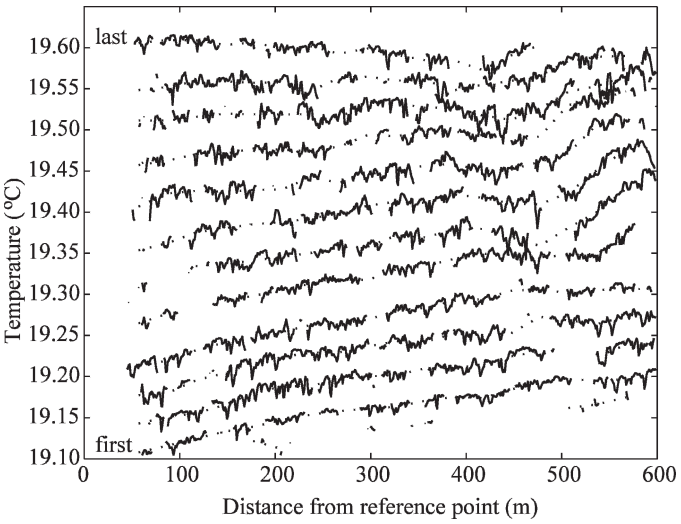

Fig. 3. Horizontal temperature measurements in the surface mixed layer: dotted lines represent 10-m bin-averaged data, and solid lines represent 1-m bin-averaged data on 09 August 2006. The first run (~20:00 h) is shown at the bottom of the figure, and the last run (~23:30 h) at the top with a transect repeat interval of ~15 min. Each profile is offset by 0.05°C for display purposes. The reference point is defined as the point where the mission was executed on the initial leg (i.e., the northeast corner of the initial transect).

smith et al. 1990) to give

$$\tilde{H} = -\rho_w C_p h \frac{\partial \overline{T}}{\partial t} \quad (1)$$

where ρ_w is density of water assumed to be 1,000 kg m^{-3}, C_p is the value of the specific heat of water (4,182 J kg^{-1} K^{-1}), h is the depth of the surface layer, and $\overline{T}$ is the layer average temperature. If we assume negligible heat flux in the horizontal ($\tilde{H}_x$) and through the base of the surface mixing layer, $\tilde{H}$ represents the heat flux across the top of the water column. Positive fluxes represent heat lost from the water to the atmosphere, driving a negative surface buoyancy flux, $B = -\beta\tilde{H}/\rho_w C_p$, where β is the buoyancy parameter defined as $\beta = g \cdot \alpha$ with g the gravitational constant and α the coefficient of thermal expansion (Wells and Sherman 2001).

$\partial\overline{T}/\partial t$ was directly estimated using $\Delta T/\Delta t$ from consecutive vertical CTD profiles as -1.7668×10^{-5} K s^{-1} and from horizontal CTD profiles at 100 m and 500 m along the mission track as (-1.4363 and -1.7758) $\times 10^{-5}$ K s^{-1}, respectively. These reported values represent the time average of $\Delta T/\Delta t$ from all repeat profiles or transects. Equation 1 was used to calculate a surface heat flux of 296 W m^{-2} from the repeated CTD vertical profiles, and 240 and 297 W m^{-2} from the two positions along the AUV transect from the horizontal CTD profiles. It should be noted that with the convention defined here, a decrease in temperature of the water column corresponds to a positive heat flux from the surface.

To test the assumption of negligible horizontal heat flux, $\tilde{H}_x$ was calculated as 0.034 W m^{-2} using an eddy diffusivity model given by $\tilde{H}_x = \rho_w C_p K_x \partial\overline{T}/\partial x$ where K_x is a horizontal eddy diffusivity taken as 0.47 cm^2 s^{-1} for a shear-free environment (Colman and Armstrong 1983) and $\partial\overline{T}/\partial x$ was approximated with a $\Delta\overline{T}/\Delta x$ of 1.73×10^{-4} W m^{-2} from the largest measured gradient (first transect) in the horizontal CTD profiles. This estimated horizontal heat flux is much smaller than the calculated vertical heat fluxes, thereby validating the neglect of horizontal heat flux in our calculations.

The estimated vertical heat fluxes are now compared to the heat flux estimated from measured meteorological data (Fig. 4). The average values for the ambient air temperature, wind speed, and relative humidity were 19.20°C, 4.35 m s^{-1}, and 40%, respectively, during the evening of 09 August 2006. With the average surface water temperature of 18.995°C, as measured by the CTD profiler, an iterative solution of the bulk aerodynamic formulae for latent (190.4 W m^{-2}) and sensible heat (-1.9 W m^{-2}) was found for the average weather characteristics over the testing period (Launiainen 1995; Launiainen and Cheng 1998; Heikinheimo et al. 1999). Since the experiment was conducted in the evening with a clear sky, both cloud cover and shortwave radiation were considered negligible for these calculations. If we sum these values with the calculated net long wave radiation (81.3 W m^{-2}) based on empirical calculations with no cloud cover (Tennessee Valley Authority 1972), the net surface heat flux rate was estimated as 270 W m^{-2}. The discrepancy between the heat flux estimated from heat content and that estimated from the meteorological data is ~25 W m^{-2}, which is within the range of accuracy observed by others (Jonas et al. 2003). It is concluded that for bulk epilimnion characterization, these three independent measures of surface heat flux are in close agreement.

It is proposed that the observed temperature gradient across the central basin results from the more extensive shallow water region along the western shore that promotes differential heating during periods of solar radiation input (Monismith et al. 1990; Lei and Patterson 2002), where shallow waters are defined as those regions whose maximum water depth is less than the solar radiation penetration depth (~30-m depth) (Lei and Patterson 2006). Slope angles, calculated from high-resolution multiangle swath bathymetry (Bird and Mullins 2005), at the base of the photic zone are 20° and 15° for the east and west sides of the lake, respectively, leading to the conclusion that there is a greater region at the west side of the lake that is exposed to periodic solar heating. The idea that variations in the accumulation of solar heat creates the observed temperature gradient across the lake is further supported by the fact that the thermal structure on 08 August 2006 (not shown) was similar to that presented for 09 August 2006 even though the average wind speed on 08 August 2006 was less at 1.42 m s^{-1} and the wind was blowing in the opposite direction (*see* Fig. 4). The implications of this basin-scale temperature gradient observed in the horizontal profiling will now be explored in greater detail.

Given sufficient time, surface heat flux will decrease background stratification until it is unstable. This well-studied process, which generates thermal instabilities in the form of convective sinking plumes, initially breaks up any residual daytime circulation patterns, promotes vertical

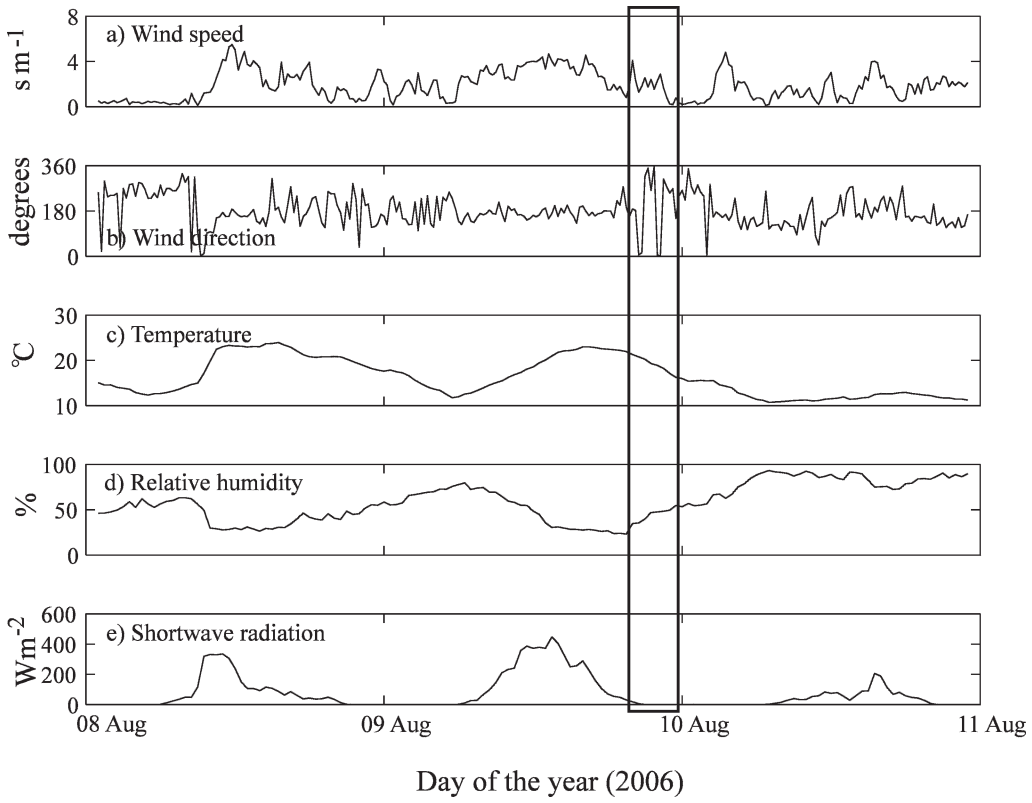

Fig. 4. Meteorological data from summertime campaign: (a) wind speed, (b) wind direction (360° represents north), (c) air temperature, (d) relative humidity, (e) incident shortwave radiation. The rectangle indicates time of AUV deployment on 09 August 2006.

mixing, and eventually establishes density currents that flow along the bottom boundaries of the lake (Horsch and Stefan 1988; Monismith et al. 1990). The two circulation patterns associated with penetrative convection (convective plumes and density currents) will be considered independently. After the system has reached steady state, the velocity scaling, v_p, of convective plumes is given by (Ward et al. 1990):

$$v_p \cong [-Bh]^{1/3} \tag{2}$$

During periods of evening cooling, the resulting negative buoyancy flux, B, was calculated from the horizontal temperature profiles to be -1.17×10^{-7} and -1.44×10^{-7} m^2 s^{-3} at 100 m and 500 m along the track, respectively. Extending the argument that the measurements on the west side of the lake represent shallower waters, this is in agreement with Fer et al. (2002*a*), who found that in Lake Geneva the magnitude of the surface buoyancy flux was greater in littoral than in pelagic waters. The calculated velocities of the fully established convective plumes were 7.7×10^{-3} and 8.3×10^{-3} m s^{-1} at 100 and 500 m along the transect, respectively. These velocities relate to associated timescales for a plume to fall from the surface to the thermocline depth of 8.7 and 8.0 min. Thus, the transect repeat time of 15–17 min was too slow to capture persistent trends in upwelling and downwelling on each pass as observed in the horizontal profiles of 1-m bin-averaged data shown in Fig. 3. However, localized temperature fluctuations larger than $\pm(2.56 \pm 0.02) \times 10^{-3}$ K (i.e., not attributably to vehicle motion) are evident on a scale of 4–8 m. It is suggested that these are further evidence of convective plumes and eddies since these are of a similar horizontal scale as seen by Thorpe et al. (1999) in the epilimnion.

Examining 1-m bin-averaged data CTD transects at 7.02-m depth (Fig. 5), two persistent features are evident. The first is the oscillatory structure seen between 100 and 200 m that is typified by transects 4, 8, and 9 of Fig. 5. While this is a potentially interesting feature, it can be attributed to vertical vehicle motion within the mean temperature gradient (i.e., on the order of 0.1°C) and will not be discussed in further detail. In contrast, in the 10-m bin-averaged data, 625 m along transect 6 (~21:45 h), there is evidence of a cold front that both persists and propagates through the remaining transects reaching a maximum intrusion position of 580 m at 23:15 h. Although sunset on 09 August 2006 occurred at 20:39 h and sunrise the next morning was at 05:57 h, the sun was off the lake by 20:00 h as a result of shading from surrounding mountains, resulting in surface cooling for 10 h. The estimated spin up time for the establishment of current patterns associated with periodically forced penetrative convection, 17–20% of the period of thermal forcing, is 100–120 min (Monismith et al. 1990; Lei and Patterson 2006). The time of onset of the observed front (~105 min from sun-off) agrees well with theory of density current formation and propagation. At this point, convective plumes are reaching the bottom of the surface layer, and there is the potential for formation of turbulent density currents in the littoral zone.

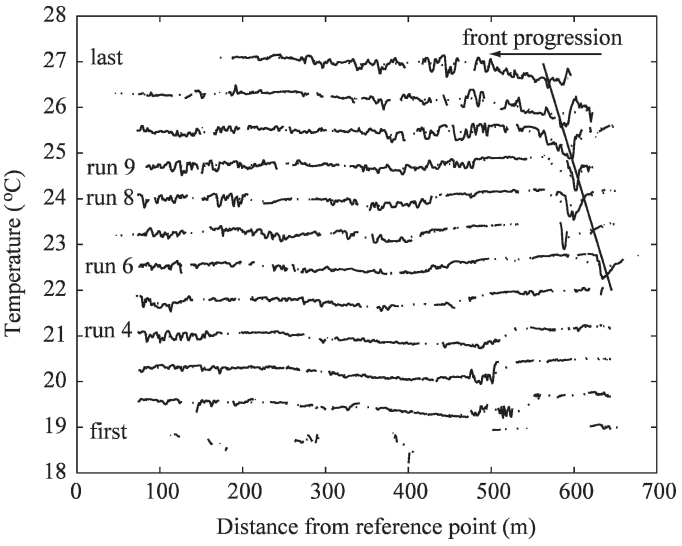

Fig. 5. Horizontal temperature measurements at the thermocline depth: dotted lines represent 10-m bin-averaged data, and solid lines represent 1-m bin-averaged data on 09 August 2006. The first run (~20:00 h) is shown at the bottom of the figure and the last run (~23:30 h) at the top with a transect repeat interval of ~15 min. Each profile is offset by 0.75°C for display purposes. The reference point is defined as the point where the mission was executed on the initial leg (i.e., the northeast corner of the initial transect).

Once formed, density currents will propagate through the surface mixed layer by running down slope in the littoral regions to the depth of the thermocline, at which point the density current may flow along the thermocline or penetrate into denser water. If penetration does result, it will have important implications for mass transport from the epilimnion to the hypolimnion. Required conditions have been experimentally quantified for both two-dimensional negatively buoyant plumes and more complex density currents to penetrate through two-layer stratification at a given depth, h, and a reduced gravity of the interface defined as $g' = g(\rho_2 - \rho_1)/\rho_0$ where ρ_1, ρ_2, and ρ_0 are the associated densities of the surface layer, bottom layer, and reference density, respectively (Ching et al. 1993; Wells and Wettlaufer 2005). The case of a two-dimensional vertical plume was characterized using a critical Richardson number defined in terms of the buoyancy flux per unit width, $\tilde{B}$:

$$Ri_\rho \equiv g' h \Big/ \tilde{B}^{2/3} \tag{3}$$

For $0.5 < Ri_\rho < 1.0$ convective plumes will penetrate the stratified interface, for $1 < Ri_\rho < 5$ plumes will spread laterally with appreciable entrainment of the underlying fluid, and for $Ri_\rho > 10$ little mixing is observed (Wallace and Sheff 1987). Although similar, the calculation of Ri_ρ for two-dimensional density currents needs to be corrected for slope geometry, slower relative velocities, and one-sided entrainment. Wells and Wettlaufer (2007) demonstrated that the critical Richardson number lies in the range of 21–27 instead of 0.5–1 and is only weakly related to slope angle.

With values for ρ_1 and ρ_2 of 998.435 ($T = 19$°C) and 999.728 ($T = 10$°C) kg m^{-3} and ρ_0 of 1,000 kg m^{-3}, g' is calculated to be 0.0126 m s^{-2}. With the mean basin width of ~500 m as an appropriate length scale for the width of the cooling water body, L, the mean $\tilde{B}$ is O(10^{-4}). The value of Ri_ρ is calculated to be 31, which is greater than the range of Ri_ρ of 21–27 required for interface penetration. In the case where the density current does not initially penetrate the stratified interface ($Ri_\rho^{in} > 27$), the surface layer evolves by the filling box mechanism of length scale, L (Baines and Turner 1969; Wells and Wettlaufer 2005). Infilling continues until the point where the reduced gravity, g', has been eroded to the critical Ri_ρ. The timescale, τ_ρ, required to achieve penetration of the thermocline, even where significant deepening is occurring, is defined by (Wells and Wettlaufer 2007)

$$\tau_\rho = \frac{\Big(\big(Ri_\rho\big)_{\text{initial}} - \big(Ri_\rho\big)_{\text{critical}}\Big) L}{\tilde{B}^{1/3}} \tag{4}$$

Both Ri_ρ and L are then used to determine a range of values for τ_ρ of 12–30 h. The implications of this are that during summer periods, nighttime cooling is generally too short for density currents, generated by surface cooling, to penetrate the thermocline. For both days of the field campaign, 08 and 09 August 2006, the temperature was above the surface water temperature for the calculated value of τ_ρ. It is acknowledged that this may not always be the case, as was demonstrated by the temperature profile on 10 August 2006 (*see* Fig. 4), where the ambient air temperature is below the surface temperature for the entire day. Density currents formed during longer cooling periods (e.g., early autumn) potentially establish flow patterns to deeper depths by penetrating the seasonal stratification.

In order to quantify the influence of the formed density currents in the pelagic regions, the concept of the entrainment ratio, E_s, is defined as the rate of increase in the density current thickness as a function of the distance down slope. This is related to a vertical plume by using an equivalent vertical entrainment constant denoted $E_q = E_s/\sin\theta$, where θ is the down-slope angle. E_q has been found to be relatively constant at 0.08 for θ less than 80° (Wells and Wettlaufer 2007), resulting in a value of E_s of 0.02 on the west side of the lake where θ equaled 15°. It has been shown that the current thickness (b) and velocity (v_{dc}) scaling equations are very similar to those of a vertical plume (Britter and Linden 1980)

$$v_{dc} = C E_s^{-1/3} \tilde{B}^{1/3} \tag{5}$$

$$b = E_s s \tag{6}$$

where s is the along slope distance above the depth of thermocline. The empirical constant C has been experimentally determined as $C = 0.2$ for slope angles in the range of 10–90° (Ellison and Turner 1959). With the previously derived scaling of $\tilde{B}$, Eq. 5 yields a predicted down-slope velocity of 0.034 m s^{-1}. This is slightly elevated in comparison with values reported for velocities associated with nighttime cooling of 0.005–0.013 m s^{-1} (Wells and

Sherman 2001) but is within range of the reported value of 0.05 m s^{-1} for the gravity current associated with the winter cascade in Lake Geneva (Fer et al. 2002*c*). Estimating the mean frontal progression of the density current along the thermocline as the rate of change of the approximate position of the temperature anomaly indicated in Fig. 5, this progression is calculated to be 0.0083 m s^{-1} over the test period. This greatly reduced velocity, relative to the predicted down-slope velocity, likely results from significant frictional dampening that occurs along the thermocline. Fer et al. (2002*c*) also reported a maximum intrusion length of 1,200 m into the 100-m deep thermocline from the Lake Geneva field study. Scaling this to the Pavilion Lake thermocline depth of 7.02 m, the expected horizontal length scale would be 80 m. The maximum distance that the cold front was recorded in the AUV data was ~150 m from the shoreline. While nearly double the expected intrusion length, the observed intrusion length is proposed to be ancillary evidence of this phenomenon occurring. The associated gravity current depth (Eq. 6) was calculated as 0.5 m, leading to the conclusion that generated density currents during nighttime cooling will have a region of influence of this height.

Wintertime campaign (radiative heat flux)—In addition to driving a negative buoyancy flux during the summer months, surface heat flux also acts as a driving force for penetrative convection under ice cover. In these conditions, where there is no mean shear, penetrative convection becomes the dominant process for mass transport in temperate lakes. The latter mechanism happens late in the winter season, after snow melt but before ice melt, when significant solar radiation can penetrate the ice. The absorption of penetrating shortwave solar radiation by the water column leads to the creation of gravitational instabilities driven by thermal forcing. Once this process has initiated, the evolving thermal structure demonstrates a self-similar four-layer structure: first, a stably stratified surface layer (SL); second, a convectively mixed layer (CL); third, an interfacial entrainment layer (EL); and, fourth, a deeper quiescent layer (QL) (Farmer 1975; Mironov et al. 2002; Jonas et al. 2003). This structure was observed in vertical CTD profiles at Pavilion Lake during February 2006 under 50 cm of lake ice (Fig. 6).

In Pavilion Lake (Fig. 6 inset) and elsewhere (c.a. Farmer 1975; Malm et al. 1997), the destabilizing buoyancy flux will have a twofold effect. The CL will deepen over time, and the overall temperature of the CL will concurrently rise. The average warming rate ($\partial \overline{T}/\partial t$ = 0.015 K d^{-1}) of this layer over the study period is an order of magnitude less than the 0.2 K d^{-1} reported by Jonas et al. (2003). The difference between these heating rates is likely due to this study being conducted early in the season, while the Lake Soppensee study (Jonas et al. 2003) was conducted days before the water column reached the temperature of maximum density (late springtime).

Detailed study of the CL is important for understanding mass transport in the water column under ice. In contrast to the surface cooling boundary problem, the radiative surface flux is distributed across the entire SL from the upper boundary of $T = 0°C$ at the ice–water interface to the lower boundary where $\partial T/\partial z = 0$ (Jonas et al. 2003). Light penetration, and the penetrative convection associated with radiative heat flux, into the water column is influenced by both the optical properties of the ice and the water column.

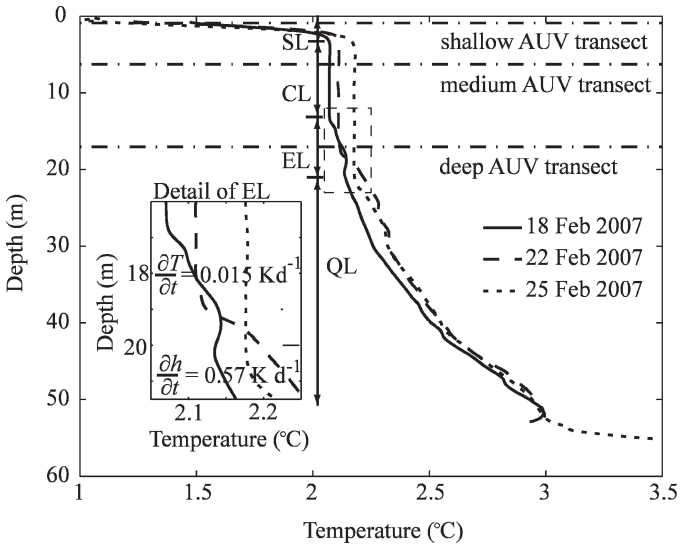

Fig. 6. Vertical CTD profiles on three separate days during the wintertime campaign demonstrating an evolving four-layer structure: surface layer (SL), convectively mixed layer (CL), entrainment layer (EL), quiescent layer (QL) (*see* inset for detail of the dashed line rectangular outlined area). Highest evidence of entrainment is evident in the first profile.

Ice thickness has greatest variability immediately after freeze-up before becoming more uniform over the course of the winter (e.g., total ice depth varies between 5 and 10 cm across the temperate Lake Vendurskoe, Russia basin by midwinter) (Bengtsson 1986; Malm et al. 1997). In contrast, ice profiles typically reveal basin-scale heterogeneity in the ratio of white to black ice. The general trend in lake ice is for white ice to radially increase from the center of the lake resulting from both wind deposition of snow on the littoral regions of the lake and decreased rates of snow melt in sunlight-sheltered areas. It has been suggested that, in late winter, sun-exposed areas of the ice will melt more quickly, resulting in variations on total ice depth of up to 10 cm (Bengtsson 1986).

In order to characterize ice thickness variability at Pavilion Lake, a total of five ice profiles were collected; three from the central basin and one each from the north and south basins. Measured ice characteristics are summarized in Table 1. There was a progression of snow and white ice from north to south, with significantly more snow in the north basin than the central basin where the central basin had wind scouring; in the south basin there was no evidence of either snow or white ice (*see* Table 1). This snow deposition pattern is typical for Pavilion Lake as given by anecdotal evidence provided by local fishermen.

Not only was there variation in white ice along the lake, but also along the AUV transect: the center of the transect (H2) has more white ice, though the conductivity of this white ice is much less (Table 1). White ice is formed from

Table 1. Lake and ice characteristics including the fraction of lake salinity (f)

	Central basin (H1)*	Central basin (H2)*	Central basin (H3)*	North basin	South basin
Measured water depth (m)	57	67	68	42	39
White ice depth (m)	0.04	0.19	0.07	0.04	0.00
Black ice depth (m)	0.46	0.21	0.46	0.24	0.30
Total ice depth (m)	0.50	0.40	0.53	0.28	0.30
Water C25† (μS cm^{-1})‡	179	181	169	—‖	—‖
White ice C25 (μS cm^{-1})§	178	63.6	161	178	n/a
Black ice C25 (μS cm^{-1})§	86.2	69.9	36.4	58.6	23.2
f, white ice	0.01	0.65	0.05	0.01	—‖
f, black ice	0.52	0.61	0.78	0.67	0.87

* H1, H2, and H3 are the three sampling sites along the AUV transect at the beginning, middle, and end of the AUV transect.
† C25 refers to the specific conductivity (i.e., conductivity normalized to 25°C).
‡ Specific conductivity measured with the YSI 556 MPS Multiprobe.
§ Specific conductivity measured from samples with the Guideline Portasal.
‖ Not measured.

combined snow and lake water that floods the ice when the weight of the snow overcomes the buoyancy of the ice sheet. That the conductivity of the white ice at the center of the lake is reduced suggests it consists of a higher proportion of snow than at the other sites. The fraction of salt excluded from the black ice also varied considerably from site to site, but is within the range of previously measured values (Pieters and Lawrence unpubl.). Field observations of cracking in the ice surface from ~0.2 to 2 m in width provide further evidence of the horizontal variability in the ice cover.

Poorly defined, the extinction of shortwave radiation in ice is highly dependent on variability in the wavelength, ice structure, and sky conditions. Launiainen and Cheng (1998) used the following approximation to estimate the surface radiation flux at the ice–water interface, $I_0(t)$, through the decay of the incident radiation in the ice column:

$$I_0(t) = (1 - \alpha_s) I_s(t) e^{-\kappa_i z_i} \tag{7}$$

where the surface albedo, α_s, was selected as 0.3 for the ice surface, $I_s(t)$ is the incident shortwave radiation, and κ_i and z_i are the extinction coefficient and ice thickness. Values of κ_i were selected as 17.1 and 8.4 m^{-1} for white and black ice, respectively, at values of z_i less than 0.1 m based on the assumption of clear skies. For z_i greater than 0.1 m, the extinction coefficients were assumed to be 1.6 and 1.5 m^{-1} for the two cases. It should be noted that the upper layer extinction coefficient would be approximately halved under cloudy skies, although becoming less important at depth as κ_i ranges between 1.4 and 1.6 m^{-1} for all cloud cover conditions below 0.1 m (Launiainen and Cheng 1998).

$I_0(t)$ then becomes the surface force driving temperature change over time, as defined in Eq. 8 (a one band parameterization of the vertical divergence of the radiation flux, $I(z, t)$, as it relates to the solar extinction coefficient in water, μ_i, that results as a buoyancy forcing; Malm et al. 1997; Jonas et al. 2003)

$$\frac{\partial T}{\partial t}(z,t) = -\frac{\partial I}{\partial z} \cong \frac{\partial}{\partial z}(I_0(t) e^{-\mu_i z}) \tag{8}$$

With Eq. 7, and the light extinction coefficients (κ_i) proposed by Launiainen and Cheng (1998), with assumed clear skies, the surface radiation flux, $I_0(t)$, is calculated to be 9.4, 6.4, and 6.9 W m^{-2} for the H1, H2, and H3 stations, respectively, in the central basin using a mean incident irradiance, $I_s(t)$, of 80 W m^{-2} measured during the test period (Fig. 7). These calculated values are close to the minimum value of 10 W m^{-2} required for convective buoyancy forcing, although they are insufficient to generate circulation patterns (Kelley 1997; Malm et al. 1997). It was noted at the time of measurement that Sta. H2 was positioned in an ice crack 2 m in width that had refrozen with white ice. This suggests that the measured ice profile was not representative of the surrounding ice cover. In contrast, it is possible to conclude that the measured total ice depth (0.40 m) was typical of the area since it matched the measured depth (0.41 m) of a nearby hole (~10 m distant). With the measured thickness and an average white ice depth of the other sites, of 0.04 m, it is possible to calculate a new increased surface radiation flux of 10.0 W m^{-2} at Sta. H2. This suggests that the center receives an increased radiative heat flux in comparison with the littoral regions.

While the destabilizing buoyancy forcing associated with solar radiation ceases with nightfall, penetrative convection continues in the CL until frictional damping dissipates the generated kinetic energy. The required time, τ_f, to damp out these convective cells is approximately equivalent to the ratio of the turbulent kinetic energy to the rate of dissipation of this kinetic energy to friction:

$$\tau_f \approx C_z \left(h^2 / \beta I(z)\right)^{1/3} \tag{9}$$

where C_z is an empirical coefficient assumed to be 0.6 (Kelley 1997), h is the depth of the CL, and $I(z)$ is defined by Eq. 8 where z is the depth of the lower boundary of the SL. $I_0(t)$ is a useful simplification for a reasonable first approximation for $I(z, t)$. This is acceptable only in the limit when the depth of the CL far exceeds the depth of the SL (Mironov et al. 2002), as is the case here. With this simplification and the length scale of the convectively mixed layer (h ~20 m during the testing period), the amount of time required to halt the motion of the convective cells, τ_f, is estimated to be ~78 min. A similar timescale of ~60 min was demonstrated for Lake Baikal (Kelley 1997). This time period is of sufficient duration to

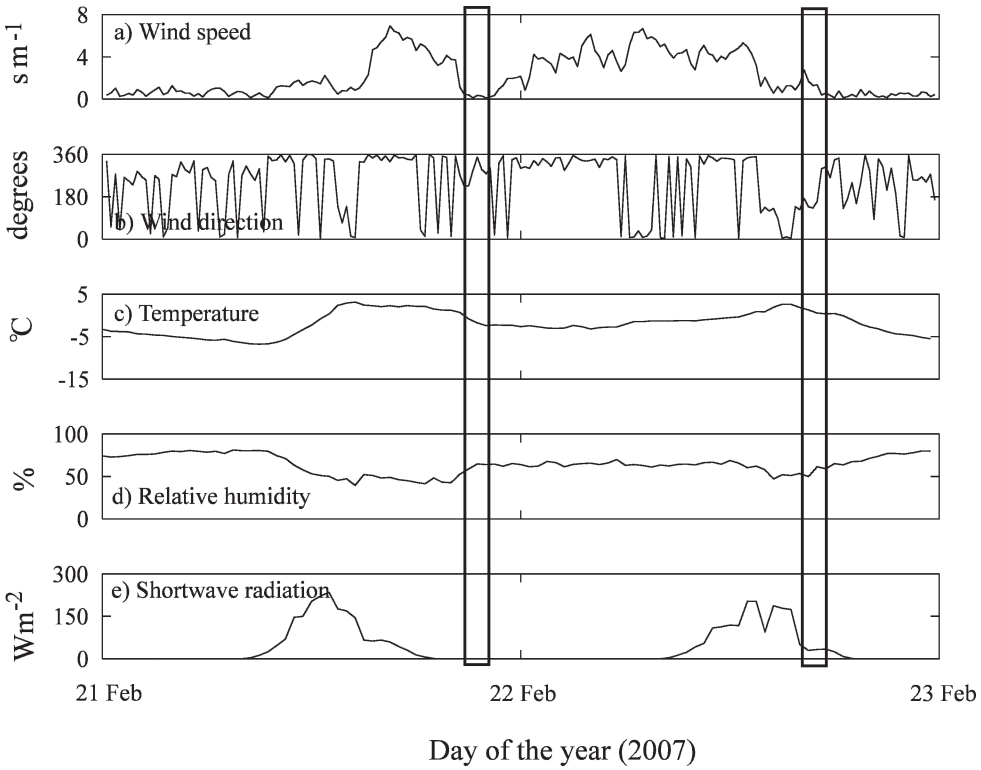

Fig. 7. Meteorological measurements during the wintertime campaign: (a) wind speed, (b) wind direction (360° represents north), (c) air temperature, (d) relative humidity, (e) incident shortwave radiation. Rectangles represent the testing periods on the two separate days.

maintain penetrative convection under scattered clouds, while not long enough to continue throughout the night.

During the winter campaign, three horizontal CTD profiles were conducted with the AUV. An evening AUV run (~21:00 h) was conducted on 21 February 2007 at a depth of 0.50 m in the surface layer (SL) only. The other two AUV runs were conducted at two depths (6.20 and 17.00 m), both in the convective layer (CL) in the late afternoon (~17:00 h) of the next day. Although sunset occurred at 17:30 h, the lake surface was in shadow after 16:30 h. With the time calculated for τ_f, convective motions should be seen on both deployments of 22 February 2007, while all motion should have been halted on 21 February 2007.

Horizontal CTD profiles in the SL on 21 February 2007 show water temperature decreasing toward the lake center (Fig. 8). The reduced temperature remains at the same location in the transect throughout the sampling period. The length scale of this region greatly exceeds the length scale of a convective cell (on order of the CL depth of 20 m), so it is unlikely to be a direct signature of convective mixing. This region likely represents variations in ice structure with an increased degree of heat transfer. (The temperature fluctuations on a scale of 2–5 m likely result from vehicle motion in the large vertical gradient (2.0 ± 0.8 K m^{-1}) in the SL temperature at the depth of the transect.)

Horizontal profiles within the CL on 22 February 2007 are shown in Fig. 9 (6.20-m depth) and Fig. 10 (17.00-m depth). In both of these figures, the 10-m bin-averaged data show the evolution of a warm temperature anomaly beneath the same central region (150–250 m from the reference point) as the cold temperature region seen in the SL (Fig. 8) the day before. The difference between the thermal regimes of these two layers (i.e., the CL and SL seem to be reflections of each other) likely results from the time of day at which the profiles were collected. Since the evening profile in the SL was conducted when ambient air temperatures were below zero, the water temperatures would be reduced in regions where the ice was thinner (i.e., toward the lake center), whereas the horizontal profiles during the afternoon would capture radiatively induced convection and circulation. Looking at the evolution of the warm temperature anomaly at the two depths in the CL, the temperature in the central region was initially close to the background value of the CL (2.12°C) on 22 February 2007 before reaching a maximum and subsequently decreasing. This suggests the evolution of a convective cell, or a series of cells, in this region. With the simplified velocity scaling of Eq. 2, the convective velocity of the gravitational instabilities would be ~1.5 mm s^{-1} with a corresponding travel time ($\tau_c = h/v_c$) of 3.7 h vertically across the CL. Since this exceeds the mission length, it is concluded that the variations seen result from the pluming action of several convective cells rather than a single one. Corroboratory evidence is provided by examining the length scales separating peaks in this region, which are ~10–25 m as demonstrated in the 1-m bin-averaged data. This is most clearly exemplified in the first and last transect of Fig. 10, where distinct peaks are present with spacing on

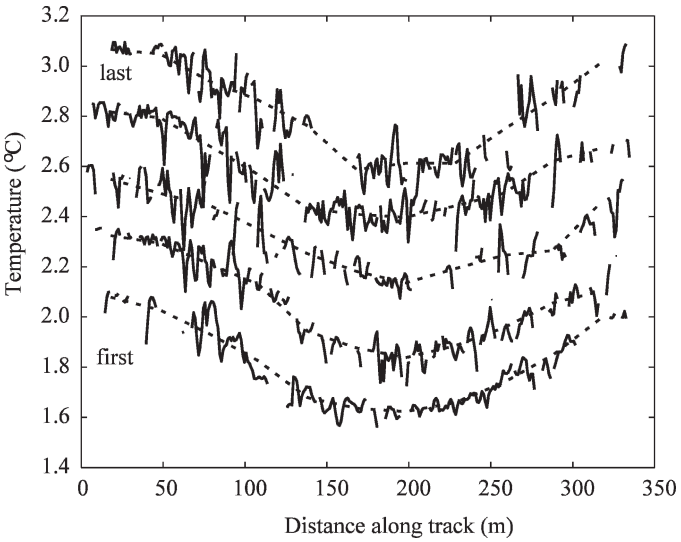

Fig. 8. Horizontal temperature measurements at the depth of the surface layer (0.50 ± 0.05 m): dotted lines represent 10-m bin-averaged data, and solid lines represent 1-m bin-averaged data on 20 February 2007. Initial run (~20:30 h) shown on bottom and final run (~21:05 h) on top yielding a transect repeat interval of ~7 min. Each profile is offset by 0.25°C for display purposes. The reference point is defined as the point where the mission was executed on the initial leg (i.e., the northeast corner of the initial transect).

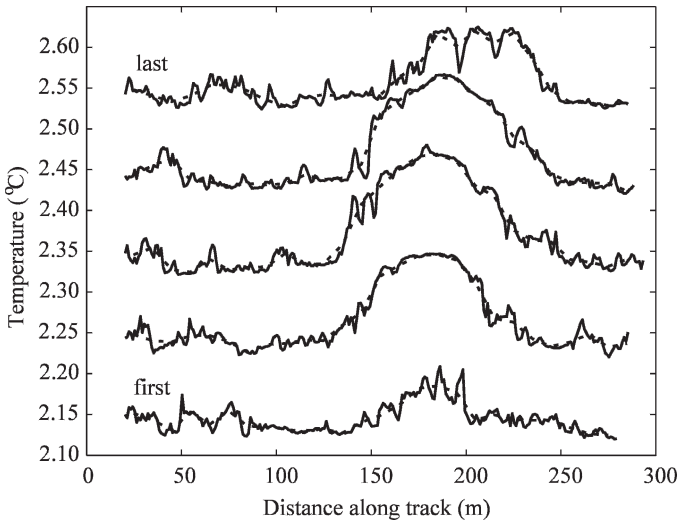

Fig. 10. Horizontal temperature measurements at 17-m depth in the convective layer: dotted lines represent 10-m bin-averaged data, and solid lines represent 1-m bin-averaged data on 21 February 2007. Initial run (~16:45 h) shown on bottom and final run (~17:20 h) on top yielding a transect repeat interval of ~7 min. Each profile is offset by 0.10°C for display purposes. The reference point is defined as the point where the mission was executed on the initial leg (i.e., the northeast corner of the initial transect).

the order of ~12 m. The possibility of water movement resulting from sediment heat flux was dismissed for two reasons: first the circulation pattern would be in the opposite direction (Welch and Bergmann 1985), and second the heat fluxes from the sediment decrease dramatically in late winter (Petrov et al. 2006).

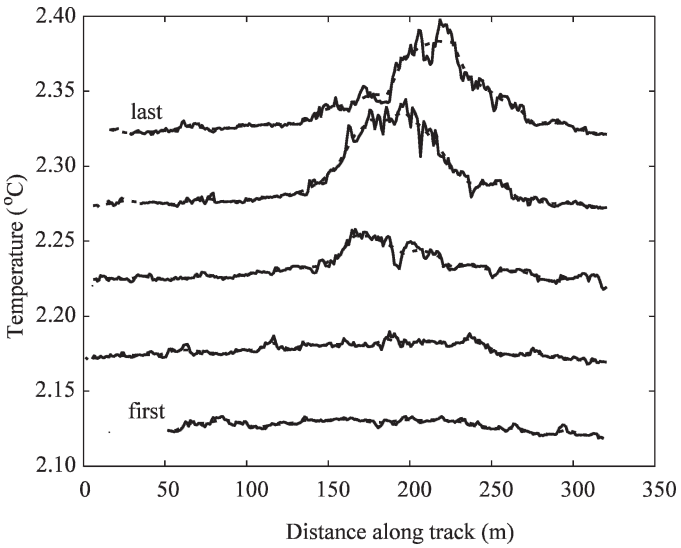

Fig. 9. Horizontal temperature measurements at 6.20-m depth in the convective layer: dotted lines represent 10-m bin-averaged data, and solid lines represent 1-m bin-averaged data on 22 February 2007. Initial run (~16:45 h) shown on bottom and final run (~17:20 h) on top yielding a transect repeat interval of ~7 min. Each profile is offset by 0.05°C for display purposes. The reference point is defined as the point where the mission was executed on the initial leg (i.e., the northeast corner of the initial transect).

Although appearing not to vary with time, there are two other features to be remarked upon in the littoral regions. In Fig. 9, the temperature at each end of the transects increases gradually toward the center, suggesting two possibilities: descending plumes are warming the surroundings through entrainment of the surrounding waters, or radiatively heated waters are collecting in the middle before initiation of a circulation pattern causing a slight overall heating. Comparing either end of the transects in Figs. 9 and 10 reveals significantly more temperature fluctuations at the 17-m depth. Although poorly understood, it is possible that these result from the generation and propagation of internal waves along the interface between the CL and the EL from the convective plumes (Farmer 1975; Kelley 1997). The EL is characterized by being stably stratified from the base of the CL to the top of the QL (*see* Fig. 6). The fact that this stratification has been shown to retain its characteristics during deepening of the CL implies that the upper and lower boundary layers of the EL will deepen synchronously during periods of convective mixing (Jonas et al. 2003). The underlying, neutrally stable QL extends from the interfacial layer to the bottom of the water column.

This work presents field observations of thermal structure formed by penetrative convection forced by a net heat flux in a quasi–shear-free environment under the following conditions: summer, nighttime cooling of the epilimnion resulting from temperature differential between the water and the air; and solar volumetric heating of the surface waters beneath the ice surface in midwinter.

Horizontal temperature profiles from both campaigns indicated that convective plumes were driving overturn within the surface waters.

During the summer, repeated horizontal temperature measurements made by an AUV suggest turbulent density currents moving from the littoral region and intruding out along the seasonal thermocline. Estimated cooling rates from the AUV-collected data were in close agreement with estimations made from both repeated CTD profiling and meteorological data. It was theorized that density current formation results from differential daytime heating of littoral water since the characteristics of an observed thermal front agreed with theory (formation time, current velocity, and intrusion length) and were independent of wind direction or speed. While further study is required to confirm this, this is a potentially important physical phenomenon driving the transport of nutrients and minerals from littoral to pelagic regions. This transport may also have implications on microbialite distribution and morphology currently being investigated in the benthos of Pavilion Lake. It is conjectured that regions subject to increased mass transport will display an increased distribution density of microbialites.

During winter, since the water temperature was below the temperature of maximum density, radiative heating rather than surface cooling was driving the observed convective pluming. This is supported by the fact that the observed thermal structure was consistent with radiative penetrative convection theory and evolved and was self-consistent over the test period. Horizontal CTD measurements suggest a region of convective circulation that was spatially heterogeneous across the lake that is proposed to result from localized optical properties of the overlying ice (e.g., total ice depth and opacity). While mass transport in this region has no direct influence on deeper waters, it highlights potential midwinter convective motion to the lake bottom in shallow areas with similar ice characteristics and affects phytoplankton communities. Additional evidence for the relation between optical properties and buoyancy flux was provided by the different depths of the convective layers in the different basins, which were correlated to the total ice depth and snow cover. This also suggests that basin-scale differences in ice cover characteristics (e.g., snow depositional pattern) drive increased levels of physical transport in the absence of mean wind shear.

In natural ecosystems, physical transport processes directly influence chemical and biological regimes (e.g., dissolved oxygen distributions, plankton population density, etc.). The eventual intent is to link these processes with the biogeochemical conditions driving microbialite formation in Pavilion Lake and other freshwater ecosystems. Physical transport is also tied closely to the fate of both conservative and nonconservative pollutants that are discharged into these environments. Understanding microscale and macroscale seasonal differences in physical transport processes is essential for environmental monitoring of both pristine and polluted lakes. While traditional limnological methods are useful for bulk characterization, this work explored previously unresolved physical dynamics of the well-mixed layer of a temperate lake in quasi–shear-free conditions that would have been difficult to quantify during summer months and impossible under winter ice cover without the use of an AUV platform.

References

Baines, W. D., and J. S. Turner. 1969. Turbulent buoyant convection from a source in a confined region. J. Fluid. Mech. **37:** 51–80.

Bengtsson, L. 1986. Spatial variability of lake ice covers. Geogr. Ann. **68A:** 113–121.

Bird, J. S., and G. K. Mullins. 2005. Analysis of swath bathymetry sonar accuracy. J. Ocean. Eng. **30:** 372–390.

Britter, R. F., and P. F. Linden. 1980. The motion of the front of a gravity current travelling down an incline. J. Fluid Mech. **99:** 531–543.

Ching, C. Y., H. J. S. Fernando, and Y. Noh. 1993. Interaction of a negatively buoyant line plume with a density interface. Dyn. Atmos. Oceans **19:** 367–388.

Colman, J. A., and D. E. Armstrong. 1983. Horizontal diffusivity in a small, ice-covered lake. Limnol. Oceanogr. **28:** 1020–1026.

Ellison, T. H., and J. S. Turner. 1959. Turbulent entrainment in stratified flows. J. Fluid Mech. **6:** 423–448.

Farmer, D. M. 1975. Penetrative convection in the absence of mean shear. Q. J. R. Meteorol. Soc. **101:** 869–891.

Fer, I., U. Lemmin, and S. A. Thorpe. 2002*a*. Observations of mixing near the sides of a deep lake in winter. Limnol. Oceanogr. **47:** 534–544.

———, ———, and ———. 2002*b*. Contribution of entrainment and vertical plumes to the winter cascading of cold shelf waters in a deep lake. Limnol. Oceanogr. **47:** 576–580.

———, ———, and ———. 2002*c*. Winter cascading of cold water in Lake Geneva. J. Geophys. Res. **106:** 3060, doi:10.1029/2001JC000828.

Fong, D. A., and N. L. Jones. 2006. Evaluation of AUV-based ADCP measurements. Limnol. Oceanogr.: Methods **4:** 58–67.

Heikinheimo, M., M. Kangas, T. Tourula, A. Venäläinen, and S. Tattari. 1999. Momentum and heat fluxes over lakes Tämnaren and Raksjö determined by the bulk-aerodynamic and eddy-correlation methods. Agric. Forest Meteorol. **98–99:** 521–534.

Horsch, G. M., and H. G. Stefan. 1988. Convective circulation in littoral water due to surface cooling. Limnol. Oceanogr. **33:** 1068–1083.

Imberger, J. 1985. The diurnal mixed layer. Limnol. Oceanogr. **30:** 737–770.

Jonas, T., A. Y. Terzhevik, D. V. Mironov, and A. Wüest. 2003. Radiatively-driven convection in an ice-covered lake investigated by using temperature microstructure technique. J. Geophys. Res. **108:** 3183, doi:10.1029/2002JC001316.

Kelley, D. E. 1997. Convection in ice-covered lakes: Effects on algal suspension. J. Plankton Res. **19:** 1859–1880.

Launiainen, J. 1995. Derivation of the relationship between the Obukhov stability parameter and the bulk Richardson number for flux-profile studies. Boundary-Layer Meteorol. **76:** 165–179.

———, and B. Cheng. 1998. Modelling of ice thermodynamics in natural water bodies. Cold Reg. Sci. Technol. **27:** 153–178.

Laval, B., J. S. Bird, and P. D. Helland. 2000*a*. An autonomous underwater vehicle for the study of small lakes. J. Atmos. Ocean. Technol. **17:** 69–76.

———, and others. 2000*b*. Modern freshwater microbialite analogues for ancient dendritic reef structures. Nature **407:** 626–629.

Lei, C., and J. C. Patterson. 2002. Unsteady natural convection in a triangular enclosure induced by absorption of radiation. J. Fluid Mech. **460:** 181–209.

———, and ——— . 2006. Natural convection induced by diurnal heating and cooling in a reservoir with slowly varying topography. Jpn. Soc. Mech. Eng. Int. J. B **49:** 605–615.

Levine, E. R., D. N. Connors, R. R. Shell, and R. C. Hanson. 1997. Autonomous underwater vehicle-based hydrographic sampling. J. Atmos. Ocean. Tech. **14:** 1444–1454.

Malm, J., A. Terzhevik, L. Bengtsson, P. Boyarinov, A. Glinsky, N. Palshin, and M. Petrov. 1997. Temperature and salt content regimes in three shallow ice covered lakes. 1. Temperature, salt content and density structure. Nord. Hydrol. **28:** 99–128.

Mironov, D., A. Terzhevik, G. Kirillin, T. Jonas, J. Malm, and D. Farmer. 2002. Radiatively driven convection in ice-covered lakes: Observations, scaling and a mixed layer model. J. Geophys. Res. **107:** 3032, doi:10.1029/2001JC000892.

Monismith, S. G., J. Imberger, and M. L. Morrison. 1990. Convective motions in the sidearm of a small reservoir. Limnol. Oceanogr. **35:** 1676–1702.

Nadis, S. 1997. Real time oceanography adapts to sea changes. Science **275:** 1881–1882.

Overnell, J., T. Brand, W. Bourgeois, and P. J. Statham. 2002. Manganese dynamics in the water column of the upper basin of Loch Etive, a Scottish fjord. Estuar. Coast. Shelf Sci. **55:** 481–492.

Petrov, M. P., A. Y. Terzhevik, R. E. Zdorovennov, and G. E. Zdorovennova. 2006. The thermal structure of a shallow lake in early winter. Water Resour. **33:** 135–143.

Stansfield, K., and others. 2001. Deep-sea, high resolution, hydrography and current measurements using an autonomous underwater vehicle: The overflow from the Straight of Sicily. Geophys. Res. Lett. **28:** 2645–2648.

Stefanovic, D. L., and H. G. Stefan. 2002. Two-dimensional temperature and dissolved oxygen dynamics in the littoral region of an ice-covered lake. Cold Reg. Sci. Technol. **34:** 159–178.

Tennessee Valley Authority. 1972. Heat and mass transfer between a water surface and the atmosphere. Tennessee Valley Authority Division of Water Resources Research, Rep. 14.

Thorpe, S. A., U. Lemmin, C. Perrinjaquet, and I. Fer. 1999. Observations of the thermal structure of a lake using a submarine. Limnol. Oceanogr. **44:** 1575–1582.

———, T. A. Osborn, J. F. E. Jackson, A. J. Hall, and R. G. Lueck. 2002. Measurements of turbulence in the upper ocean mixing layer using Autosub. J. Phys. Oceanogr. **33:** 122–145.

Wallace, R. B., and B. Sheff. 1987. Two-dimensional buoyant-jets in two-layer ambient fluid. J. Hydraul. Eng. Am. Soc. Civil Eng. **113:** 992–1005.

Ward, P. R. B., K. J. Hall, T. G. Northcote, W. Cheung, and T. Murphy. 1990. Autumnal mixing in Mahoney Lake, British Columbia. Hydrobiologia **197:** 129–138.

Welch, H. E., and M. A. Bergmann. 1985. Water circulation in small arctic lakes in winter. Can. J. Fish. Aquat. Sci. **42:** 506–520.

Wells, M. G., and B. Sherman. 2001. Stratification produced by surface cooling in lakes with significant shallow regions. Limnol. Oceanogr. **46:** 1747–1749.

———, and J. S. Wettlaufer. 2005. Two-dimensional density currents in confined basins. Geophys. Astrophys. Fluid Dyn. **99:** 199–218.

———, and ———. 2007. The long-term circulation driven by density currents in a two-layer stratified basin. J. Fluid Mech. **572:** 37–58.

Received: 20 August 2007
Accepted: 2 February 2008
Amended: 9 March 2008